Chinese Journal of Aeronautics, (2015), 28(3): 749–756

Chinese Society of Aeronautics and Astronautics
& Beihang University

Chinese Journal of Aeronautics

cja@buaa.edu.cn
www.sciencedirect.com

A study of instability in a miniature flying-wing aircraft in high-speed taxi

Song Lei, Yang Hua *, Yan Xufeng, Ma Cong, Huang Jun

School of Aeronautic Science and Engineering, Beihang University, Beijing 100191, China

Received 21 July 2014; revised 25 November 2014; accepted 12 February 2015
Available online 9 April 2015

KEYWORDS

Dynamic analysis;
Flying wing;
Stability;
Takeoff;
Taxiing

Abstract This study investigates an instability that was observed during high-speed taxi tests of an experimental flying-wing aircraft. In order to resolve the reason of instability and probable solution of it, the instability was reproduced in simulations. An analysis revealed the unique stability characteristics of this aircraft. This aircraft has a rigid connection between the nose wheel steering mechanism and an electric servo, which is different from aircraft with a conventional tricycle landing gear system. The analysis based on simulation results suggests that there are two reasons for the instability. The first reason is a reversal of the lateral velocity of the nose wheel. The second reason is that the moment about the center of gravity created by the lateral friction force from the nose wheel is larger than that from the lateral friction force from the main wheels. These problems were corrected by changing the ground pitch angle. Simulations show that reducing the ground pitch angle can eliminate the instability in high-speed taxi.

1. Introduction

Several next-generation civil transport aircraft and unmanned air vehicles (UAVs) are of flying-wing designs. Flying-wing aircraft have potential benefits over conventional configurations in aerodynamic and structural efficiency.[1] Many UAVs use the flying-wing configuration because it minimizes the observability of the aircraft while meeting flight performance requirements.[2] Over the last decade, flight tests have been conducted on flying-wing aircraft such as the X-45,[3–5] and the X-48B[6–8] from Boeing and the X-47B[2,9,10] from Northrop Grumman. Because flying-wing aircraft have no vertical tails, the lateral-directional dynamics and the directional control of these aircraft differ from those of conventional aircraft. These differences affect both the flying qualities and the stability of ground maneuvers.

A number of studies have been conducted to establish a mathematical model for aircraft runway dynamics.[11–17] In particular, several studies[11–13] considered the effects of the aerodynamic forces while taxiing. Abzug[11] replicated the 1935's demonstration of the tricycle landing gear arrangement effect on light aircraft directional stability in landing rollout by computer simulation. Zhang and Zhou[12] studied the takeoff run for a flying-wing aircraft and considered both the aerodynamic

* Corresponding author. Tel.: +86 10 82317915.
E-mail addresses: strikerlei@126.com (L. Song), yhbuaa@163.com (H. Yang), yxflame@163.com (X. Yan), macong513@163.com (C. Ma).
Peer review under responsibility of Editorial Committee of CJA.

ELSEVIER Production and hosting by Elsevier

http://dx.doi.org/10.1016/j.cja.2015.04.001

forces and the ground loads. Evans et al.[13] presented the development of a tricycle landing gear simulation model including several classes of system failures such as component degradation and jamming. Zhang and Nie[14] established a mathematical model of aircraft wheel braking and nose wheel steering, and studied landing gear strut loading during steering and braking control. Gu and Gao[15] established the dynamic model of landing gear shimmy, and analyzed directional stability during taxi by using this model. Ro[16] presented a descriptive modeling to study aircraft-runway dynamics, which is descriptive and structured in the sense that landing gear system is regarded as an assembly of suspension strut, tire, and wheel. Pi et al.[17] developed a generic aircraft ground operation simulation to predict the response of aircraft under various operating modes and surface conditions. In summary, although in many studies, mathematical model of aircraft ground dynamics has been established and the taxi maneuver has been simulates in several aspects, rare of them consider that aircraft design characters caused abnormal behavior study, and less of them concerns about taxing stability from the standpoint of aircraft design.

This study examines an instability phenomenon observed in a small experimental aircraft with a flying-wing configuration while taxiing at high speed. The cause of the problem is determined by examining the aerodynamic and structure mechanism of the experimental aircraft. Based on the results of the analysis, a mathematical model of instability is developed and the problem is reproduced in simulations. A solution to the problem is found by integrating the results from the analysis and the simulation. After validating the solution in the simulation, a flight test of the modified aircraft is performed and high-speed taxi stability is demonstrated.

2. Presentation of problem

This study examines the stability and control of a small experimental aircraft with a flying-wing configuration. Fig. 1 presents an overhead view of the aircraft, which has a takeoff weight of 34.3 N, a wing area of 1.13 m^2, a tip washout angle of $-3°$ and a wing loading of 3.1 kg/m^2. Propulsion is provided by an electric-powered ducted fan with a maximum takeoff thrust of 20 N. The engine thrust line passes through the center of gravity (C.G.) of the aircraft. The trailing edge control surfaces, from the tip to the root, are the split drag rudders, the elevons and the elevators. This aircraft does not have flaps

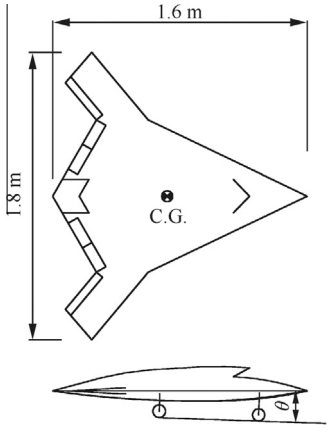

Fig. 1 Planform and side views of aircraft.

or other high-lift devices. In the plane of symmetry, the center of gravity is 0.88 m from the nose and 7% MAC (mean aerodynamic chord, MAC = 0.93 m) in front of the aerodynamic center of the aircraft.

The landing gear configuration of the experimental aircraft resembles that of the large majority of small aircraft of similar weight and size. The landing gear struts are constructed from steel wire and the tires are polyurethane. To simplify the structure, the nose gear does not include a shimmy damper and the steering mechanism of the nose wheel is directly connected to an electric servo. The horizontal distance between the center of gravity and the main gear is 0.05 m and the distance to the nose gear is 0.58 m. The center of gravity is 0.15 m above the ground. There is no toe-in angle for the wheels on the main landing gear. This aircraft uses both nose wheel steering and split drag rudders to control the direction while taxiing and in takeoff runs. In order to reduce the takeoff run distance, the aircraft has a ground pitch angle of 4° (the angle between the chord line and the runway surface, shown in Fig. 1 as θ).

When taxiing, all of the control surfaces initially remained neutral. When taxiing at low speed, the overall control of the aircraft was normal. However, in high-speed taxi trials a strange instability emerged. When the aircraft was disturbed even slightly in the yaw direction, such as by a side force on the nose wheel due to an uneven surface or a steering correction by the pilot, the aircraft performed a ground loop; i.e., the aircraft turned dramatically in the direction of the disturbance, leading to a heading change of greater than 180° over a short distance. Because this ground loop happened suddenly and the yaw rate increased rapidly, the pilot was unable to control it. Figs. 2(a)–(g) show sequential images of the instability, graphically shown in Fig. 2(h).

There are certain differences in the characteristics of ground loops with this aircraft and conventional taildragger aircraft. Taildragger aircraft are prone to ground loops while taxiing at low speed. As the taxi speed increases, the yawing moment from the vertical tail increases and improves directional stability. In contrast, the experimental aircraft was prone to ground loops while taxiing at high speed. A preliminary analysis eliminated the possibility that a structural asymmetry or pilot error caused the ground loop.

The ground loop problem also occurs in the aircraft shown in Fig. 3. The aircraft in Fig. 3 has a landing gear configuration similar to that of the aircraft in this study but is somewhat different in shape. The display of similar ground loop behavior indicates that the problem may be universal in small flying-wings.

A preliminary theoretical analysis indicates that the ground loop behavior is caused by the following two factors:

(1) The rigid connection between the nose wheel steering mechanism and an electric servo causes the load distribution to differ from that of a conventional tricycle landing gear configuration during takeoff run. Generally, ground loops are unlikely in aircraft with a tricycle landing gear configuration. The nose gear in aircraft with a typical tricycle landing gear layout usually features a shimmy damper. In these aircraft, the nose wheel can automatically turn in the direction of the velocity if the aircraft sideslips during takeoff run. The nose gear in many small aircraft with a tricycle landing gear layout resemble that of the aircraft in this study

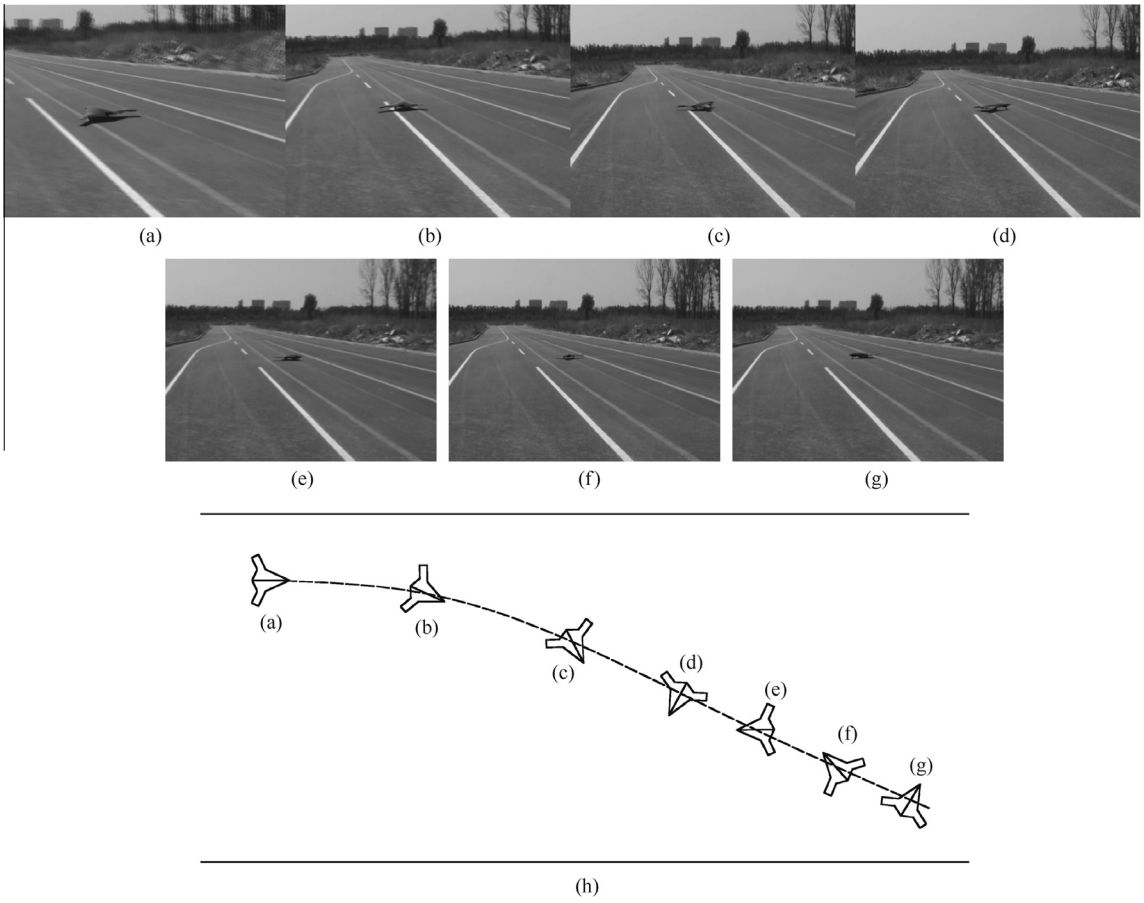

Fig. 2 Directional instability of aircraft in high-speed taxi.

Fig. 3 A different aircraft with a similar ground loop problem.

in that there is no shimmy damper and the steering mechanism for the nose wheel is directly connected to an electric servo. Thus, the nose wheel cannot automatically turn in the direction of motion during takeoff run. This difference could make the load distribution different from that of a conventional tricycle landing gear layout during takeoff run.

(2) Aerodynamic forces may contribute to the ground loops. The reason lies in that the aircraft behaves normally when taxiing at low speed and becomes unstable when making steering corrections at high speed.

3. Foundation of dynamic model

The coordinate systems used in the analysis are the earth-fixed frame ($o_E x_E y_E z_E$) and the body-fixed frame ($o_b x_b y_b z_b$), both of which use the right-hand rule. The origin of the earth-fixed frame is located at the initial position of the taxiing aircraft. The positive x_E-axis is directed in the initial heading of the taxiing aircraft, the positive z_E-axis is directed downward (toward the ground) and the y_E-axis is perpendicular to the plane $x_E o_E z_E$ with the positive direction directed toward the right side of the aircraft. The origin of the body-fixed frame is located at the center of gravity of the aircraft. The x_b-axis is in the plane of symmetry and the positive direction is toward the nose of the aircraft, parallel to the wing root chord line. The z_b-axis is in the plane of symmetry, perpendicular to the x_b-axis and positive downward. The positive y_b-axis is directed toward the right side of the aircraft. Fig. 4 presents the free body diagram for the force and moment analysis for taxiing and the relevant parameters. The diagram depicts the positive senses of the forces and moments, where P_{mL} and P_{mR} denote the support forces from the ground to the left and right main landing gears; A_n and A_m, the distance between the center of gravity and the nose or main wheel in the side view; F_{Sm} and F_{Sn}, lateral friction suffered by the nose wheel and the main wheels; u and v, the aircraft velocity components along the x_b and y_b axes; u_n and v_n, the nose wheel longitudinal and lateral velocities relative to the ground; u_m and v_m, the main wheel longitudinal and lateral velocities relative to the ground. P_n denotes the support forces from the ground to the nose gear, G the aircraft weight, T the thrust, φ_p the angle between engine thrust line and x_b-axis, H_{CG} the height of the center of gravity from the ground during taxiing, ε the steering angle of the nose

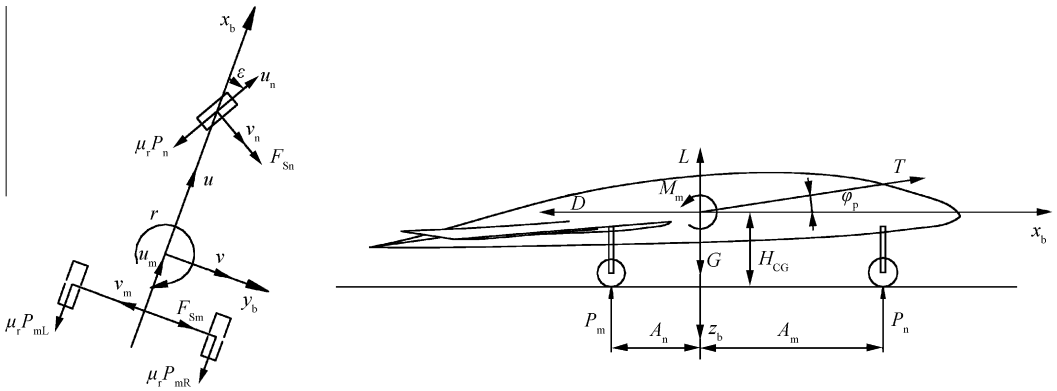

Fig. 4 Forces and parameters for dynamic model of taxiing aircraft.

wheel, μ_r the rolling friction coefficients of the landing gear wheels and r yawing angular velocity.

The aircraft in this study uses steel wire struts and polyurethane wheels for the landing gear. The landing gear of large aircraft uses oleo-pneumatic shock-absorbing struts and biasply tires, so the analysis methods used for large aircraft may be inappropriate in this case. Intuitively, the deformations of the landing gear and the tires are small while taxiing, and a qualitative analysis suggests that the occurrence of ground loops has little relationship with the deformation of the struts and the wheels. Therefore, to simplify the computations the struts and the wheels are assumed to be rigid. The ground loop phenomenon reproduced in simulations validates this assumption. The aerodynamic forces are assumed to be linear in the simulation model. Because the linear model is accurate over a limited range, the simulation is terminated when the sideslip angle exceeds a certain value.

The forces are described as follows. In the following equations, L, D and Y denote aerodynamic lift, drag and side force respectively; L_m, M_m and N_m denote the rolling moment, pitching moment and yawing moment respectively; B denotes the distance between the left and right main wheels, and J_z the aircraft moment of inertia in yaw; x_E and y_E denote the coordinates of the aircraft center of mass relative to earth-fixed axes; ψ denotes the aircraft heading angle.

While taxiing and during a ground loop, all of the wheels were in constant contact with the ground. The aircraft forces were considered to be balanced in the vertical direction and the moments were balanced in the pitch and roll axes.

$$P_n + P_{mL} + P_{mR} = G - L - T\sin\varphi_p \tag{1}$$

$$\begin{aligned} &A_n P_n - A_m P_{mL} - A_m P_{mR} \\ &-\mu_r H_{CG} P_n \cos\varepsilon - \mu_r H_{CG} P_{mL} \\ &-\mu_r H_{CG} P_{mR} - H_{CG} F_{Sn}\sin\varepsilon = -M_m \end{aligned} \tag{2}$$

$$\frac{B}{2}P_{mL} - \frac{B}{2}P_{mR} = -L_m \tag{3}$$

Because the magnitude and the direction of the lateral velocities of the left and right main wheels are the same, the lateral friction forces acting on the two main wheels were simplified as one force. This force was considered to act at the intersection point of the line connecting two main wheels axis and the symmetry plane. The rotation about the yaw axis (z-axis) is given by

$$\begin{aligned} &-A_n\mu_r P_n \sin\varepsilon + A_n F_{Sn}\cos\varepsilon \\ &-A_m F_{Sm} - J_z\frac{dr}{dt} = -N_m \end{aligned} \tag{4}$$

The acceleration of the center of gravity in the x_b-axis is given by

$$\begin{aligned} &-\mu_r P_n\cos\varepsilon - \mu_r P_{mL} - \mu_r P_{mR} - F_{Sn}\sin\varepsilon \\ &-m\frac{du}{dt} = D - T\cos\varphi_p - mvr \end{aligned} \tag{5}$$

The acceleration of the center of mass in the y_b-axis is given by

$$\begin{aligned} &-\mu_r P_n\sin\varepsilon + F_{Sn}\cos\varepsilon + F_{Sm} - m\frac{dv}{dt} \\ &= mur - Y \end{aligned} \tag{6}$$

The equations of motion were used to obtain the lateral velocities of the nose and the main wheels:

$$v_n = -u\sin\varepsilon + v\cos\varepsilon + rA_n\cos\varepsilon \tag{7}$$

$$v_m = v - A_m r \tag{8}$$

The velocity in the earth-fixed frame was calculated using the expressions in Eq. (9). These equations were used to calculate the motion of the aircraft center of mass while taxiing.

$$\begin{cases} \dfrac{d\psi}{dt} = r \\ \dfrac{dx_E}{dt} = u\cos\psi - v\sin\psi \\ \dfrac{dy_E}{dt} = u\sin\psi + v\cos\psi \end{cases} \tag{9}$$

The rolling and sliding friction forces of the wheels were computed assuming that the wheels were rigid and using measured values for the friction coefficients. To describe the change of the lateral friction forces of the wheels from static to kinetic, the friction was calculated using the following simplified method. According to the basic formula used to calculate friction, the maximum lateral static friction force acting on at the wheel was determined as

$$F_{Sx.\max} = \mu_s P_x \quad (x = n, m) \tag{10}$$

where $F_{Sx.\max}$ represents the maximum lateral friction force provided by the surface and P_x the normal force exerted by the wheels on the ground. The subscript x refers to "n" and "m", which denote the nose wheel and the main wheels, respectively. The force F_S is the minimum friction force required for the wheels to roll without sideslip while taxiing.

When $F_S < F_{S.max}$, the friction force is set to F_S; when $F_S > F_{S.max}$, the friction force is set to $F_{S.max}$ with the same direction as F_S. μ_s denotes the lateral static friction coefficient of the landing gear wheels. For a nonzero lateral velocity, the friction force is determined as

$$F_{Sx} = \mu_k P_x \tag{11}$$

where μ_k denotes the lateral kinetic friction coefficient of the landing gear wheels. The lateral friction force acts in the opposite direction of the lateral velocity of the wheel, and this is true for both the main and nose wheels.

4. Simulation of instability

To verify the equations of motion, a numerical simulation was constructed in the MATLAB programming environment. Table 1 shows the main parameters of the aircraft used for the simulation. In which $C_{l\beta}$, $C_{n\beta}$ and $C_{y\beta}$ denote the aircraft sideslip derivatives, C_{nr} denotes the aircraft damping in yaw derivative. The aerodynamic data in Table 1 were obtained from an analysis using the vortex lattice method[18,19], and the ground effect was introduced in the aerodynamic model through image-vortex theory.[20] The zero lift drag was obtained by the Raymers component buildup method.[21] The friction coefficient used in the simulation was measured with a simple measuring system consisting of a wood frame with four wheels, a ticker-tape timer and a sloped concrete surface, as shown in Fig. 5. The wheels on the frame were the same as those used on the experimental aircraft. By varying the slope and using the ticker-tape timer to determine the acceleration, the friction coefficients were determined. The values obtained for the rolling friction coefficient μ_r, the dynamic lateral friction coefficient μ_k and static lateral friction coefficient μ_s were 0.078, 0.820 and 0.824, respectively.

The only control input for the aircraft was the steering angle of the nose wheel; there were no deflections of the control surfaces. To simulate steering corrections made by the pilot, a positive 10° nose wheel steering angle (i.e., 10° to the right) was input over an interval of 0.6 s. To simplify the computations, the input was assumed to be an impulse function. Because a linear aerodynamic model was used, the simulation is terminated when the sideslip angle exceeds 30° to guarantee the accuracy of the calculations. In addition, the model assumes that all three wheels remain in contact with the ground, so the simulation is terminated if the vertical force on a strut becomes zero.

Steering inputs were given at speeds of 3 m/s and 7 m/s to simulate taxiing at low and high speeds. The dynamic responses for the two cases are shown in Fig. 6 and the loads on the landing gear are shown in Fig. 7. The two vertical dashed lines in each plot indicate the beginning and the end of the steering input. The variable N_f plotted in Fig. 7 is the moment generated by the lateral friction forces from the main wheels and the nose wheel about the center of gravity, which is given by

$$N_f = A_m F_{Sm} - A_n F_{Sn} \tag{12}$$

Table 1 Main parameters of aircraft in simulation.

Parameter (unit)	Value	Parameter (unit)	Value
J_Z (kg.m^2)	0.7045	$C_{l\beta}$ (rad^{-1})	−0.0255
C_L	0.1300	$C_{n\beta}$ (rad^{-1})	0.0010
C_D	0.0108	C_{nr} (rad^{-1})	−0.0018
C_m	−0.0123	$C_{y\beta}$ (rad^{-1})	0.0009

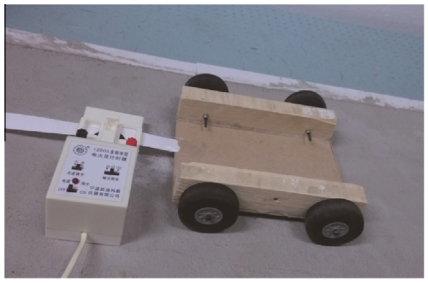

Fig. 5 System for measuring friction coefficients of wheels.

It can be observed from the response for the low-speed case in Fig. 6(a) that there are two sudden changes in the lateral velocity of the nose wheel, which correspond to the beginning and the end of the steering input. The lateral velocity of the nose wheel decrease to 0 m/s gradually after end of steering adjustment. However, the lateral velocity of the main wheels remains constant at 0 m/s for the entire maneuver. A slipping velocity of the center of gravity occurs while heading adjustment. The lateral velocity of the center of gravity and the yaw rate increase gradually after the deflection of the nose wheel, and when the deflection angle of the nose wheel returns to 0°, the lateral velocity and the yaw rate also decrease to zero. The change in the heading angle over the entire maneuver is 36° to the right. It can be observed in the landing gear loads (Fig. 7(a)) that with taxiing speed increasing, the vertical force on the nose gear increase continuously, and the vertical force on the main landing gear decrease continuously. The direction of the lateral friction force of the nose wheel change once, at the end of the steering input, and that of the main wheel remain constant. After the deflection angle of the nose wheel returns to 0°, N_f remain positive, causing the yaw rate of the aircraft to decrease to 0 rad/s.

For the high-speed case shown in Fig. 6(b), the two steps in the lateral velocity of the nose wheel occur as before. However, a skidding velocity of the center of gravity occurs while heading adjustment. As the deflection angle of the nose wheel returns to 0°, the lateral velocity of the nose wheel decreases below 0 m/s and its direction reverses, i.e., turns to the left. After ending the steering input, the lateral velocity of the main wheels increase gradually, which suggests a sideslip to the left. The trend for the change in the lateral velocity of the center of gravity is similar to that of the main wheels. However, the yaw rate initially decreases after the end of steering input but then increases and diverges. The simulation shown in Fig. 6(b) is terminated when the angle of sideslip reached 30°, which is the limit of the linear aerodynamic model, as explained previously. When the simulation reaches the criterion of the termination, the change in the heading has been greater than 81°. The angle of sideslip reaches its limit less than 1 s from the end of the steering input. This result indicates that the divergence happens quite fast. From the loads on the landing gear shown in Fig. 7(b), the trend in the vertical forces on the nose and main landing gear are as same as those in Fig. 7(a). It is notable by combing Figs. 7(a) and (b), that the direction reverses of the lateral friction acting on nose wheel, the direction reverse of the lateral velocity on nose wheel, and the

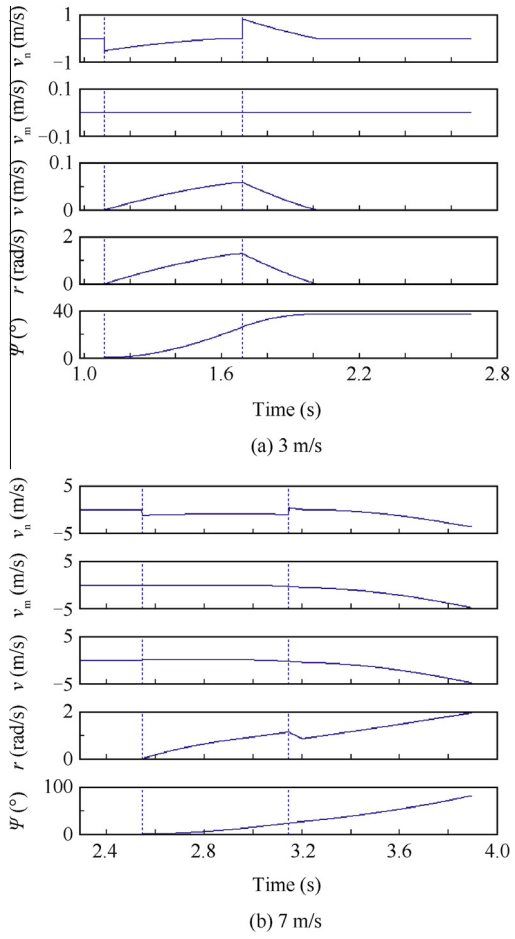

Fig. 6 Response of taxiing aircraft to a steering input at two speeds: 3 and 7 m/s.

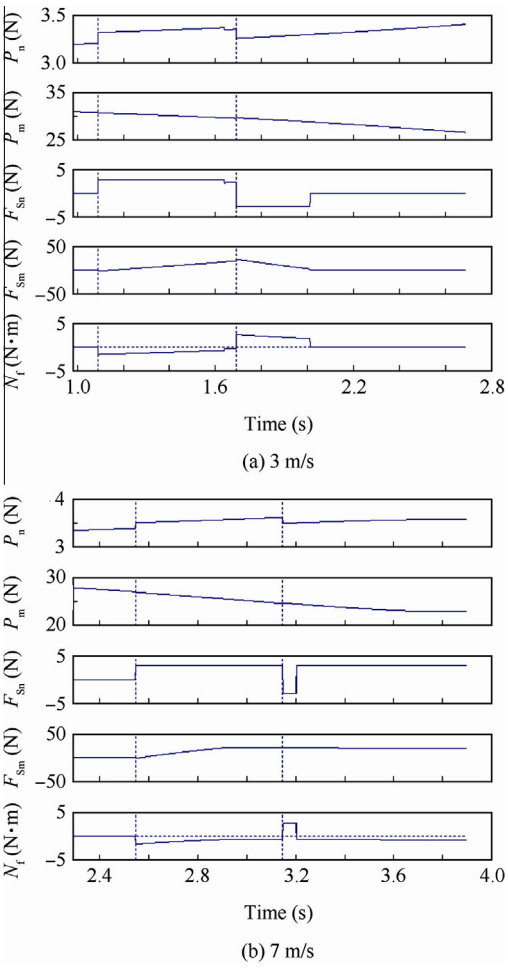

Fig. 7 Loads on landing gear caused by a steering input at two speeds: 3 and 7 m/s.

yawing divergence appears in the same time. Before the end of the steering input, a positive N_f causes the decrease of yaw rate. When the lateral velocity of the nose wheel is reversed, N_f becomes negative, causing the instability.

5. Analysis of mechanics of directional instability

The simulation results indicate that there are two main conditions necessary to produce the directional instability: the first is the reversal in the lateral velocity of the nose wheel, and the second is that the moment about the center of gravity from the lateral friction force of the nose wheel is greater than that from the lateral friction force of the main wheels.

It can be observed from Fig. 6(b) that the starting point of the yawing divergence corresponds to the time when the direction reverses on the lateral velocity of the nose wheels. From Fig. 8, it can be observed that a lack of lateral friction during heading adjustment causes skidding velocity on both nose and main wheels. At the time of yawing divergence, the aircraft has both the motion of translation and rotation. For the main wheels, the direction of the velocity $\boldsymbol{v}_{rm}$ is as same as the direction of lateral velocity $\boldsymbol{v}$, while the $\boldsymbol{v}_{rm}$ is the lateral velocity induced by yawing on main wheels. The lateral friction force acting on main wheels inhibited the yaw and the sideslip, because its direction is opposite to the directions of both $\boldsymbol{v}$ and $\boldsymbol{v}_{rm}$. In contrast, $\boldsymbol{v}_{rn}$, the induced velocity by yawing at nose wheel position has an opposite direction with lateral velocity $\boldsymbol{v}$. The vector sum of $\boldsymbol{v}_{rn}$ and $\boldsymbol{v}$ determines the direction of the friction force of the nose wheel. A special situation arises when $\boldsymbol{v}$ is relatively large: the lateral friction force of the nose wheel has a same direction as $\boldsymbol{v}_{rm}$, which produces a moment about the center of gravity that prone to increase the yaw rate. This situation corresponds to the divergence of the yaw rate shown in Fig 6(b).

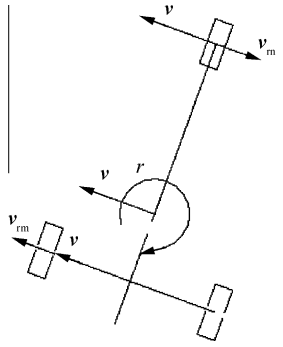

Fig. 8 Lateral velocities of nose and main wheels while turning.

In addition to the coincidence described above, there is another condition required for the occurrence of the directional instability. This second condition is that the moment about the center of gravity created by the lateral friction force of the nose wheel is greater than the moment create by the lateral friction acting on main wheels.

Under the conditions of ignoring the pitching effective generated by the aerodynamic forces, the thrust and the rolling friction, the vertical forces on the nose and main wheels are as same as the parking situation. They are respectively given by

$$P_{\mathrm{n}} = \frac{A_{\mathrm{m}} G}{A_{\mathrm{m}} + A_{\mathrm{n}}} \tag{13}$$

$$P_{\mathrm{m}} = \frac{A_{\mathrm{n}} G}{A_{\mathrm{n}} + A_{\mathrm{m}}} \tag{14}$$

If the nose and main wheels sideslip to the same direction as described previously, from Eqs. (11)–(14) it follows that

$$\begin{aligned} N_{\mathrm{f}} &= A_{\mathrm{m}}\mu_{\mathrm{k}}P_{\mathrm{m}} - A_{\mathrm{n}}\mu_{\mathrm{k}}P_{\mathrm{n}} \\ &= \frac{\mu_{\mathrm{k}}A_{\mathrm{m}}A_{\mathrm{n}}G}{A_{\mathrm{n}} + A_{\mathrm{m}}} - \frac{\mu_{\mathrm{k}}A_{\mathrm{m}}A_{\mathrm{n}}G}{A_{\mathrm{n}} + A_{\mathrm{m}}} = 0 \end{aligned} \tag{15}$$

Thus, when the lateral velocity of the nose wheel reverses, as the sum of the moments due to the lateral friction forces on the nose and main wheels about the center of gravity goes to zero, the aircraft is at the critical condition for yaw divergence. In reality, just as the aerodynamic forces create a nose-down pitching moment (Table 1), the rolling friction forces on the wheels also generate a nose-down pitching moment. As the taxiing speed increases, the aerodynamic forces increase, the vertical force on the nose wheel increases and the vertical forces on the main wheels decrease (refer to P_{n} and P_{m} in Figs. 7(a) and (b)). At this time, when the lateral velocity of the nose wheel reverses, the higher force on the nose wheel causes N_{f} to rapidly become negative, and thus the yaw rate diverges.

Based on the simulation results and the analysis, it could be inferred that to avoid the yaw instability in taxi, two actions are required. The first is to increase the lateral friction forces of the wheels while heading adjustment that prevent unfavorable sideslip on landing gear wheels, thus avoiding a reversal in the lateral velocity of the nose wheel. The second is to change the pitching moment, thus reducing the vertical force on the nose wheel and increasing the vertical force on the main wheels while taxiing to prevent an adverse yawing moment if the lateral velocity of the nose wheel reverses.

Given these two requirements, reducing the ground pitch angle is a simple and effective method to solve the yaw instability in high-speed taxi. The decrease in ground pitch angle reduces the angle of attack while taxiing, thus reducing the aerodynamic lift and increasing the vertical forces on the nose and main wheels. The increase in the vertical forces generates larger lateral friction forces on the wheels, which inhibit sideslip of the wheels. In addition, given that the aircraft in this study is longitudinally statically stable, reducing the angle of attack increases the pitching moment, which reduces the vertical force on the nose wheel. Thus, even if the lateral velocity of the nose wheel reverses, because the moment generated by the friction force of the nose wheel about the center of gravity is larger, the convergence of the yaw rate is guaranteed. Based on the preceding analysis, the ground pitch angle was changed to 2°, and the response to a nose wheel deflection of 10° to the right in 0.6 s at a speed of 7 m/s was simulated. The relevant main aerodynamic parameters are shown in Table 2, and the time histories of the states and the landing gear loads are shown in Fig. 9. It can be observed from Fig. 9 that the yaw rate decreases to zero after approximately 0.2 s as the nose wheel steering angle returns to zero. That is to say, the results of numerical simulation indicate that reducing the aircraft ground pitch angle is an effective approach for preventing ground loops.

Several flight tests conducted on the aircraft shown in Fig. 1 have proved that this method could effectively solve the instability problem of the aircraft during high-speed taxi operations. Using the same method, the ground loop problem of the aircraft shown in Fig. 3 was also solved.

Because the takeoff rotation speed is mainly determined by the stall speed, the decrease in the ground pitch angle has little

Table 2 Main parameters of aircraft with a reduced ground pitch angle.

Parameter (unit)	Numerical	Parameter (unit)	Numerical
J_Z (kg.m^2)	0.7045	$C_{l\beta}$ (rad^{-1})	−0.0064
C_L	0.0225	$C_{n\beta}$ (rad^{-1})	0.0012
C_D	0.0092	C_{nr} (rad^{-1})	−0.001
C_m	0.0041	$C_{y\beta}$ (rad^{-1})	0.0009

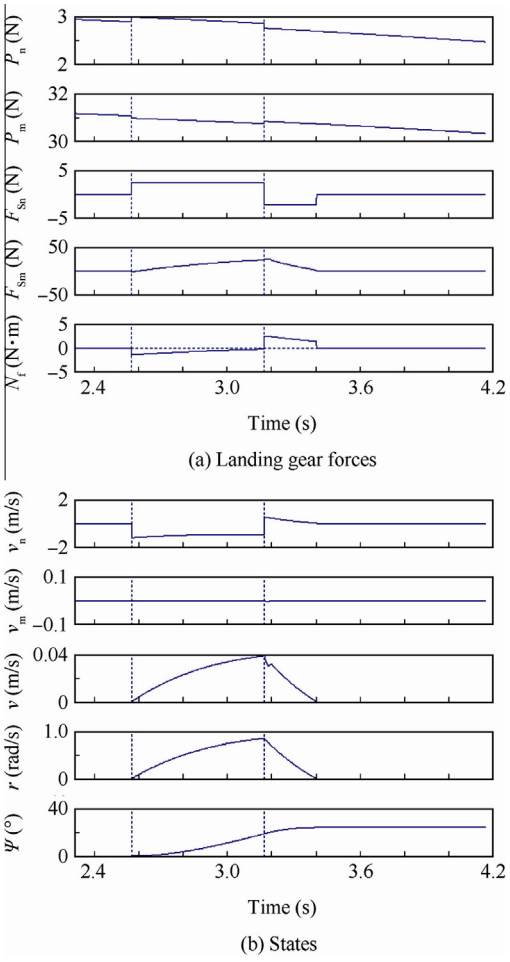

Fig. 9 Response of taxiing aircraft with a reduced ground pitch angle to a steering input.

influence on the rotation speed. Because a smaller ground pitch angle increases the time required for the nose wheel to rotate to the takeoff angle of attack, the takeoff distance will increase slightly. Although a smaller ground pitch angle increases the takeoff distance somewhat, this change is nevertheless required for safety reasons.

For the aircraft with larger dimension and higher wing loading such as a full-scale aircraft, if it has static longitudinal stability and rigid connection between the nose wheel steering mechanism and an electric servo, larger ground pitch angle may cause the instability during high speed taxi as described in this paper. In consideration of the difference between the tire of full-scale aircraft and miniature aircraft, the ground friction calculation method described in this paper may reduce the precision if used in the case of full-scale aircraft. But it is still feasible in conceptual design to roughly estimate whether the aircraft will be instable in high-speed taxi.

6. Conclusions

In this study, we investigate a kind of instability phenomenon in a small, flying-wing aircraft that occurs while taxiing at high speeds. A mathematical model was developed, and the instability was reproduced in simulations. After analyzing the simulation results, it was decided that reducing the ground pitch angle would be an effective method to solve the instability problem. The simulation results and the force analysis indicate that:

(1) The aircraft ground pitch angle has a profound impact on the stability when taxiing at high speeds, especially for a flying-wing aircraft with a rigid connection between the nose wheel steering mechanism and an electric servo.
(2) For a flying-wing aircraft with a rigid connection between the nose wheel steering mechanism and an electric servo, there are two main conditions that create an instability while taxiing: the first is a reversal of lateral velocity of the nose wheel, and the second is that the moment about the center of gravity generated by the lateral friction force of the nose wheel is greater than that of the lateral friction forces of the main wheels.
(3) For a longitudinally stable aircraft with a similar landing gear configuration, by reducing the ground pitch angle to reduce lift while taxiing, the lateral friction forces of the wheels can be increased to inhibit sideslip of the wheels. In addition, the nose-up pitching moment generated by the reduced ground pitch angle guarantees that the yaw rate converges when the lateral velocity of the nose wheel reverses.
(4) The simulation strongly indicates that the tendencies of flying-wing aircraft with similar landing gear configurations to exhibit ground loops could be reduced by changing the ground pitch angle. Flight test results support this conclusion.

References

1. Bolsunovsky AL, Buzoverya NP, Gurevich BI, Denisov VE, Dunaevsky AI, Shkadov LM, et al. Flying wing problems and decisions. *Aircr Des* 2001;**4**:193–219.
2. Whittenbury JR. *Configuration design development of the Navy UCAS-D X-47B*. Reston (VA): AIAA; 2011. Report No.: AIAA-2011-7041.
3. Wise KA. *X-45 program overview and flight test status*. Reston (VA): AIAA; 2003. Report No.: AIAA-2003-6645.
4. Wise KA. *First flight of the X-45A unmanned combat air vehicle (UCAV)*. Reston (VA): AIAA; 2003. Report No.: AIAA-2003-5320.
5. Davidson RW. *Flight control design and test of the joint unmanned combat air system (J-UCAS) X-45A*. Reston (VA): AIAA; 2004. Report No.: AIAA-2004-6557.
6. Risch T, Cosentino G, Regan CD. *X-48B flight-test progress overview*. Reston (VA): AIAA; 2009. Report No.: AIAA-2009-0934.
7. Regan CD. *In-flight stability analysis of the X-48B aircraft*. Reston (VA): AIAA; 2008. Report No.: AIAA-2008-6571.
8. Vicroy DD. *Blended-wing-body low-speed flight dynamics: summary of ground tests and sample result*s. Reston (VA): AIAA; 2009. Reprot No.: AIAA-2009-0933.
9. Wood D. X-*47A pegasus flight and mission systems design and test*. Reston (VA): AIAA; 2003. Report No.: AIAA-2003-6628.
10. Perry JD. *Navy unmanned air systems 1915–2011*. Reston (VA): AIAA; 2011. Report No.: AIAA-2011-6948.
11. Abzug MJ. *Directional stability and control during landing rollout*. Reston (VA): AIAA; 1998. Report No.: AIAA-2474-0439.
12. Zhang HL, Zhou Z. Modeling and direction-controlling for flying-wing UAV in ground motion. *J Syst Simul* 2008;**20**(24):6759–62 Chinese.
13. Evans P, Perhinschi MG, Mullins S. *Modeling and simulation of a tricycle landing gear at normal and abnormal conditions*. Reston (VA): AIAA; 2010. Report No.: AIAA-2010-7618.
14. Zhang M, Nie H. Dynamics analysis of aircraft ground steering and braking responses. *Acta Aeronaut Astronaut Sin* 2008;**29**(3):616–21 Chinese.
15. Gu HB, Gao ZJ. Landing gear shimmy and directional stability of aircraft undergoing non-straight taxiing. *Chin J Aeronaut* 2001;**14**(2):73–7.
16. Ro K. *A descriptive modeling and simulation of aircraft-runway dynamics*. Reston (VA): AIAA; 2003. Report No.: AIAA-2003-1895.
17. Pi WS, Yamane JR, Smith MJC. *Generic aircraft ground operations*. Reston (VA): AIAA; 1986. Report No.: AIAA-1986-0989.
18. Thomas M. *A vortex lattice MATLAB implementation for linear aerodynamic wing applications* dissertation. Stockholm, Sweden: Department of Aeronautical and Vehicle Engineer, Kungliga Tekniska Högskolan (KTH); 2000.
19. Katz J, Plotkin A. *Low-speed aerodynamics*. 2nd ed. Cambridge: Cambridge University Press; 2001. p. 340–51.
20. Hoak DE, Finck RD. *USAF stability and control DATCOM, AFWAL-TR-83-3048, 4.7.1 Ground effect on lift variation with angle of attack*. OH: Air Force Wright Aeronautical Laboratory, Wright-Patterson AFB; 1960 (revised 1978).
21. Raymer DP. *Aircraft design: a conceptual approach (AIAA Education Series)*. 2nd ed. Reston (VA): AIAA; 1992. p. 281–5.

Song Lei received the B.S. and M.S. degrees from Beihang University in 2008 and 2010 respectively, and is now a Ph.D. candidate. His main research interests are aircraft conceptual design and optimization.

Yang Hua received the B.S. degree from Beihang University in 2010, and is now a Ph.D. candidate. His main research interests are aircraft conceptual design and optimization.

Huang Jun is a professor in Beihang University. His main research interests are aircraft conceptual design, aircraft low-observability design and aircraft operation effectiveness analysis.